The 600–800-mb Minimum in Tropical Cloudiness Observed during TOGA COARE

PAQUITA ZUIDEMA

Program in Atmospheric and Oceanic Sciences, University of Colorado, Boulder, Colorado

(Manuscript received 7 January 1997, in final form 10 October 1997)

ABSTRACT

A minimum in cloud coverage occurring between 800 and 600 mb can be inferred from soundings taken within the tropical western Pacific warm pool. Surface observations of clouds and satellite-derived outgoing longwave radiation values suggest that the cloud minimum in the 600–800-mb layer occurs in all weather conditions. One explanation for the enhanced occurrence of clouds above (in the 400–600-mb layer) and their diminished occurrence within the 600–800-mb layer is a preferential cloud detrainment from convection into the more stable levels existing at pressures below 600 mb and above 800 mb. This mechanism is supported by the results of a buoyancy-sorting model.

1. Introduction

Tropical clouds manifest a rich complexity in their shapes and vertical distribution, ranging from the cumulonimbus and cirrus anvils that typify disturbed conditions to the trade wind cumuli of fairweather conditions. Quantitative observations of the vertical cloud distribution are very difficult to obtain. Conventional satellites only sense the cloud tops (and upper layers) and surface observers primarily notice cloud bases (and lower layers). Midlevel clouds, while common, are particularly difficult to observe and quantify. This problem is exacerbated in the Tropics by the depth of the troposphere and the complexity of the vertical distribution of the cloud systems (e.g., Sheu et al. 1997). Radar and lidar have begun to provide more realistic cloud structure descriptions (e.g., Rickenbach and Rutledge 1998). Another method for inferring the vertical location of cloud layers is from radiosonde-derived relative humidity profiles (e.g., Wang and Rossow 1995). Mapes and Zuidema (1996) used such a technique to infer a minimum in clouds in the 600–800-mb layer in the tropical western Pacific. Initially, it was the slight minimum in the mean equatorial relative humidity profile at around 700 mb (Fig. 1) that suggested a possible corresponding cloudiness minimum.

A cloudiness minimum at the 700-mb level will influence the radiative and latent heating profile of the tropical atmosphere, which in turn will affect the dynamics at both small scales (e.g., Ramaswamy and Ramanathan 1989) and large scales (Randall et al. 1989; Sherwood et al. 1994). Ultimately, understanding the complicated interactions between tropical clouds and the larger-scale environment requires documentation and explanation of the observed cloud structure, including the cloudiness minima at 700 mb. One mechanism affecting tropical cloud vertical distribution can be the lateral entrainment and detrainment of air from convective clouds. Modeling studies show that cloud detrainment occurs preferentially into layers of higher static stability (Bretherton and Smolarkiewicz 1989; Ferrier and Houze 1989; Taylor and Baker 1991; Raymond and Wilkening 1982). Within such layers, a decrease in buoyancy with height will inhibit a rising parcel from further movement upward and promote cloud formation at that level. Observationally, this may perhaps be seen in the ''altocumulus formed by the spreading out of cumulus,'' the most frequently occurring middle cloud type in the tropical region studied here (Table 2). Mapes and Zuidema (1996) observe a vertical distribution for tropical dry layers similar to the distribution inferred here for clouds, and speculate that stable layers at the base of (tropical) dry layers are also preferred regions for midlevel cloud decks. This speculation forms the basis of the investigation presented here.

We utilize about 2900 soundings to infer the cloud vertical distribution. These soundings were collected at the sites listed in Table 1 as part of the TOGA COARE (Tropical Ocean Global Atmosphere Coupled Ocean–Atmosphere Response Experiment; see Webster and Lukas 1992), conducted over the tropical western Pacific ocean during the boreal winter of 1992–93. A collocation of these soundings with satellite infrared brightness temperatures demonstrates that the minimum in cloudiness at 700 mb occurs independent of the prevailing weather. Analysis of the surface cloud obser-

Corresponding author address: Paquita Zuidema, Program in Atmospheric and Oceanic Sciences, University of Colorado, Campus Box 311, Boulder, CO 80309.
E-mail: zuidema@monsoon.colorado.edu

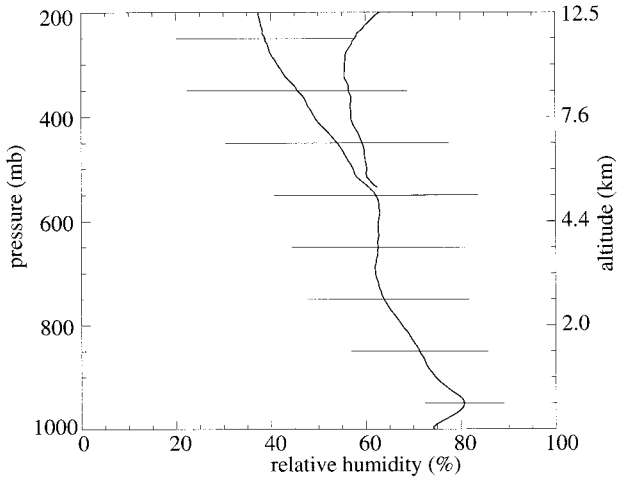

FIG. 1. Mean relative humidity profile for November 1992 through Febuary 1993 using all sounding sites listed in Table 1, both with respect to water and with respect to ice. The horizontal bars indicate two standard deviations.

vations for the same location and time of year as the soundings, but covering a 40-yr time span, illustrates the connections between midlevel cloud and overall convection. Finally, the buoyancy-sorting model of Raymond and Blyth (1992) is used to investigate a hypothesized cause for the 600–800-mb cloud minimum.

2. Analysis of soundings

a. Data

During the TOGA COARE Intensive Observation Period (IOP), four land sites and four ship sites launched four soundings per day for about four months each (see Parsons et al. 1994). Early problems noted in the near-surface humidity values, caused by sensor-arm heating or cooling at launch, have been corrected for (Miller 1993). Efforts at humidity corrections are still on going. The data are interpolated to the evenly spaced 5-mb pressure level data we rely on for this analysis (Miller 1993). The sonde relative humidity (RH) values are measured with respect to water; at temperatures below 0°C, the relative humidity with respect to ice (RH_{ice}) is subsequently calculated using the formulation of Flatau et al. (1992).

The relative humidity sensor, the Vaisaila Humicap thin film capacitor, has a stated accuracy of ±2% relative humidity. Previous studies have shown that such sensors can have a low RH bias in clouds (e.g., Garand et al. 1992). The sondes used here incorporate a new algorithm promising more accurate measurements at high humidities, but humidity underestimates and radiational heating errors can still occur (Nash et al. 1995; Betts et al. 1995). At cold temperatures, sensor icing and a long sensor response time (Paukkunen 1995) diminishes the reliability of the relative humidity values. This will not affect our results as the cloudiness minimum we focus on is located at above-freezing temperatures. Soundings containing more than 20% missing or bad data are excluded (about 5% of the soundings); these soundings were generally launched under severe weather conditions, so that a slight ''fairweather'' bias is incorporated into the final usable dataset of about 2790 soundings (out of 2900 total).

TABLE 1. Locations of the sounding sites used within this study.

Kavieng (island)	3°S, 151°E
Kapingamarangi (island)	1°N, 154°E
Kexue 1 (ship)	4°S, 156°E
Shiyan 3 (ship)	2°S, 158°E
Moana Wave (ship)	2°S, 156°E
Xiangyanghong 5 (ship)	2°S, 155°E
Nauru (island)	0.5°S, 167°E
Manus (island)	2°S, 147°E

Data from a vertically pointing laser ceilometer (White et al. 1995) present on the *Moana Wave* are also used. The ceilometer, operating at a 904-nm wavelength, has a maximum vertical range of 3480 m, and the final data has a vertical resolution of about 100 m. We use the median cloud base inferred during a 30-s time period. During times of precipitation, cloud base is obscured and no cloud base values are available.

b. Relative humidity threshold selection

Surface cloud observations are often used to validate cloud amounts derived through other methods (e.g., Rossow and Garder 1993; Wang and Rossow 1995). In the Tropics, clouds can possess large aspect ratios, and surface observers will report a cloud coverage of the celestial dome that exceeds the cloud area projected normally to the earth's surface. This helps explain the large disparity between the low-altitude cloud amount measured by surface observers (50%) and that measured by a vertically pointing ceilometer (19%). Instead of surface observations, we choose to use ceilometer-derived cloud amounts to establish a relative humidity cloud-proxy value, because the radiosonde and ceilometer sample similarly. Both instruments are vertically directed and both ignore very thin clouds. Neither instrument functions well in precipitating conditions, when cloud bases are obscured to the ceilometer and radiosondes are more likely to fail. Our method is simple: one relative humidity threshold value indicates cloud or clear conditions.

A comparison between all the available ceilometer and sounding RH data (Fig. 2) arrives at a value of 93% for the RH cloud proxy. To put the ceilometer and sounding RH measurements in the same context, both are shown as cumulative frequency distributions of inferred cloud. The figure represents a ''bottom-up'' integral, in which the cumulative cloud cover increases only if profiles that are cloud free at a lower altitude detect cloud at a higher altitude. Moisture at pressures greater than 980 mb is ignored. At altitudes above 800

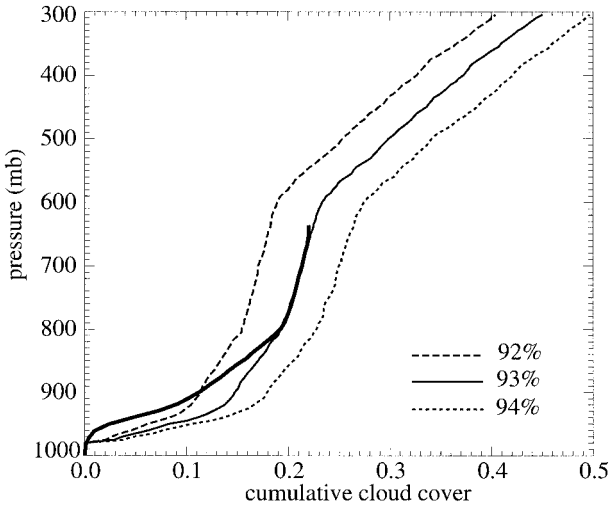

FIG. 2. Cumulative frequency distribution of cloud cover as a function of height, as seen from the surface. The dotted, solid, and dashed lines refer to the 92%, 93%, and 94% RH thresholds, respectively. Thick solid line is cloud fraction as deduced by the ceilometer. Relative humidities at pressures >980 mb are ignored.

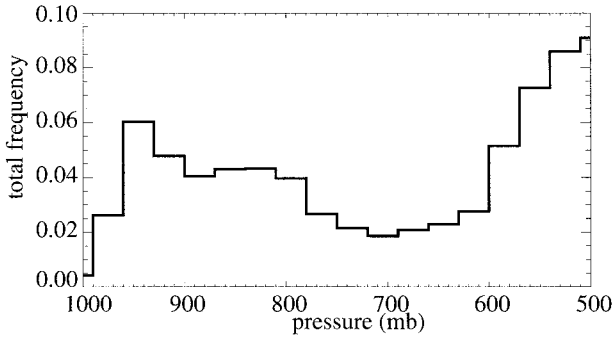

FIG. 3. Total frequency of cloud occurrence at each level (cloud amount within each 30-mb bin divided by the total number of soundings in the data sample), estimated using a 93% RH threshold.

mb, the ceilometer cumulative cloud cover is well approximated by the sounding cloud cover deduced using a 93% relative humidity threshold. Deduced cloud amount is very sensitive to the relative humidity threshold chosen, with about a 0.04 increase in total cloud amount for a 1% decrease in relative humidity threshold. Conversely, the ceilometer cloud amount would need to err by 0.04, or 20% of the total, before our choice of RH cloud proxy would be affected. The threshold choice is not sensitive to the discrepancy between the ceilometer and the sonde existing at low altitudes (not shown).

Several limitations exist to this methodology. At altitudes below 800 mb the ceilometer and sonde infer clouds more disparately. This reflects the existence of moist yet cloud-free near-surface sounding layers and the lack of ceilometer data during times of precipitation. The determination that all layers with RH values greater than 92% are cloudy suggests that the sondes still possess a dry bias. In a comparison of the RH-derived and ceilometer cloud base distributions, the maximum cloud base frequency occurs at around 930 and 950 mb for the ceilometer and soundings, respectively, independent of the RH threshold used. The ceilometer cloud bases occur most frequently slightly above the lifting condensation level of near-surface air (White and Fairall 1996) while the RH-derived cloud bases are most frequent near the top of the near-surface mixed layer (Johnson and Dickey 1996). Ultimately, the strength of the (inexact) correspondence between the optimum RH threshold and a real level-by-level cloud proxy is unclear. A more complex method is not justified. Most important to this paper is that the results are independent of the RH threshold chosen.

c. Inferred cloud characteristics

Figure 3 shows the frequency of occurrence of the very high relative humidity layers serving as a cloud proxy. A mean cloud amount at each vertical level is derived by dividing the number of ''cloudy'' layers by the total number of soundings. Results for pressures less than 500 mb are uncertain and are not shown. The figure is a very clear indicator that fewer clouds occur between 750 and 600 mb, or between 2.5 and 4.5 km. About one-half of the total cloud ($p < 500$ mb) occurs at pressures greater than 700 mb, with a peak in the distribution at about 950 mb and a smaller peak at about 830 mb. After that a distinct minimum in cloud frequency occurs from about 750–600 mb followed by a sharp increase in cloud occurrence at pressures less than 600 mb. Layers with 100% relative humidity follow a similar vertical distribution.

A compositing of the sounding data by their collocated satellite infrared brightness temperatures (Fig. 4) shows that the inferred cloud minimum is present independent of the prevailing weather. The minimum infrared brightness temperatures from the Japanese Geosynchronous Meteorological Satellite occurring within 1 h of the sonde launching time and within a 0.5° by 0.5° box centered on each sounding site are used; these serve as an independent meteorological indicator. The soundings are then subdivided into four brightness temperature quartiles, with the boundaries occurring at 221, 244, and 273 K. A reduced cloud amount between 600 and 800 mb can be inferred for the three colder quartiles. The warmest quartile, as can be expected, does not contain much cloud at all at pressures less than 750 mb. The coldest quartile corresponds the most closely to deep-convective conditions [a 208-K threshold provides a more stringent convection proxy (e.g., Chen et al. 1996) and generates a similar cloud occurrence distribution as the 221-K threshold]. The coldest quartile contains substantially more *total* midlevel cloud than the other three quartiles and also manifests a pronounced and broad *relative* minimum at 700 mb. This implies that (a) the generating mechanism for at least some of

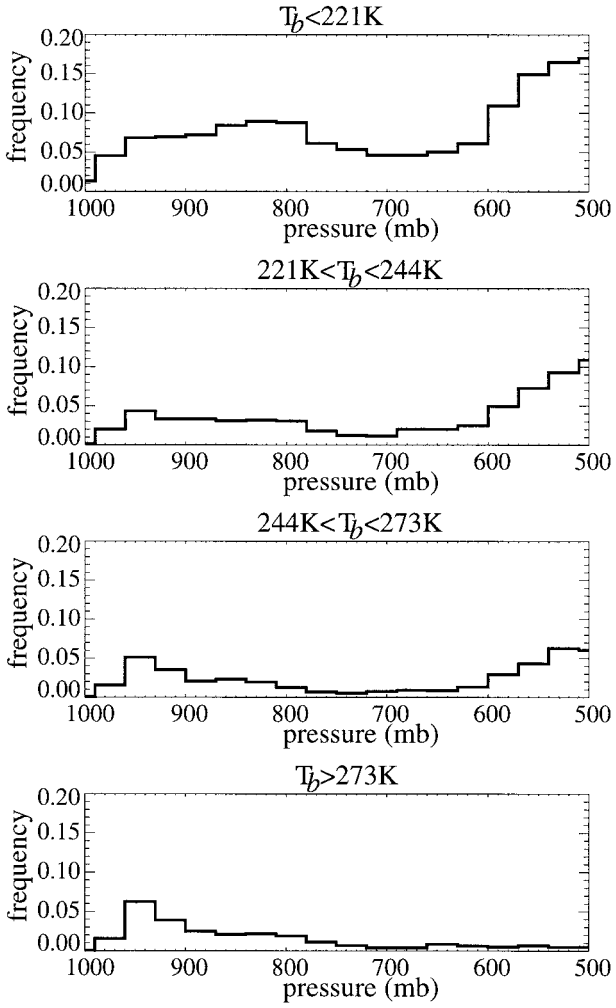

FIG. 4. Frequency of cloud occurrence binned by infrared brightness temperature T_b. Bin separations occur at T_b values of 221, 244, and 273 K. Each bin contains roughly 350 soundings.

the midlevel cloud is convection, and (b) convection preferentially avoids forming cloud material in the 600–800-mb layer in favor of lower and upper levels.

3. Surface cloud observations

Surface observations can also be used to investigate whether the existence of tropical midlevel cloud is linked to a deep convective source. We use a dataset of individual synoptic weather reports that provide information on the individual cloud types (Hahn et al. 1994). Such marine reports have formed the basis of the cloud climatologies presented in Hahn et al. (1982) and Warren et al. (1988). The dataset spans from 1954 until 1992, and only November–February observations falling within 3°N–5°S and 150°–160°E are used, or 16 588 surface observations in total. About 80% of these were taken during the day and the rest during moonlit nighttime. The surface reports distinguish between nine different cloud types at each of three vertical levels, with the clouds classified according to the height of the cloud base. Midlevel clouds lie between 800 and 380 mb, so that the 600–800-mb layer is not articulated separately. Table 2 lists the nine low and middle cloud types, as well as their diurnal-mean frequency of occurrence and amount for the location and time period stipulated here.

The middle cloud types themselves do not suggest their originating mechanism, aside from the most frequent type, ''altocumulus formed by the spreading out of cumulus,'' which also contributes the most to the total midlevel cloud cover. Several other aspects of the surface observations point to a convective source for midlevel cloudiness, however. One is that the amount and frequency of occurrence of middle cloud within this region of deep convective activity is much higher than the respective global averages of 28% and 52% for ocean areas (Warren et al. 1988).

TABLE 2. First column states the individual low cloud type, followed by its diurnal-mean cloud-type frequency of occurrence and amount. The three highest frequencies and amounts are given in bold. The last three columns are similar to the first three but pertain to middle clouds. The last row states the frequency of occurrence and average amount for any low cloud type and any middle cloud type. Frequency of occurrence refers to how often a cloud type is seen anywhere within the celestial dome, while the cloud amount is the product of the frequency of occurrence and the cloud amount when that cloud type is present, estimated in oktas.

Low cloud type	Freq.	Amount	Middle cloud type	Freq.	Amount
Fair weather cumulus (Cu)	**17.3**	5.4	thin altostratus (As)	**7.4**	3.6
Cu of considerable development	**28.0**	**10.7**	thick As	6.7	4.4
Cumulonimbus (Cb) with ill-defined top	**16.0**	**7.7**	thin altocumulus (Ac), one level	**11.5**	**4.6**
Stratocumulus (Sc) from spreading of Cu	6.8	4.2	thin Ac, two levels	9.5	2.9
Sc not formed by Cu	5.9	4.4	thin Ac, thickening	6.0	3.2
Stratus (St) and fracto St, not bad weather	3.3	2.8	Ac formed by the spreading out of Cu	**12.3**	**5.0**
Bad weather fracto St and Cu	4.7	4.0	thick or double-layered Ac	7.1	**4.8**
Cu and Sc, bases at different levels	8.4	**6.1**	Ac with turrets	3.1	1.1
Cb with cirriform top	7.1	4.0	Ac of a chaotic sky	4.4	2.2
Any low cloud type	97.6	49.3	any middle cloud type	75.0	43.0

TABLE 3. Frequencies of cloud co-occurrence. P(al : b) denotes the probability of cloud type ''a'' given the presence of cloud type ''b''. Midlevel cloud includes nimbostratus and assigns a frequency of occurrence of 0.84 to midlevel cloud that is obscured by lower cloud. Only daytime cloud observations are used; nighttime probabilities are similar but always slightly lower, perhaps reflecting a remaining diurnal observer bias. Cumulus refers to the low cloud types defined in the first two rows in Table 2, stratus+stratocumulus to rows 4–8, and cumulonimbus to rows 3 and 9.

P(mid : low)	0.77
P(mid : Cu)	0.67
P(mid : St)	0.88
P(mid : Cb)	0.85

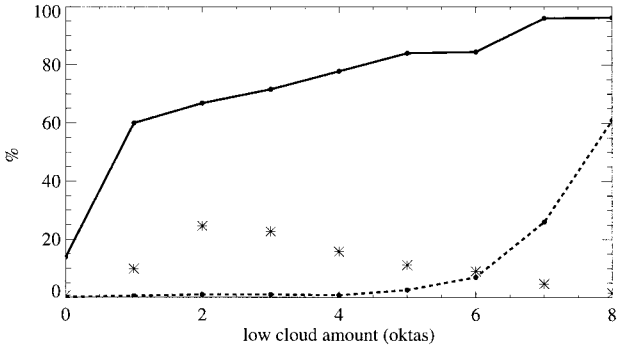

FIG. 5. Solid line denotes the middle cloud frequency of occurrence as a function of the low cloud amount. Asterisks mark what percentage of the total sample (11 852 observations) contributed to the middle cloud frequency calculation at that low cloud amount. Dashed line indicates what percentage of all observations with middle cloud reported as missing, occurred at that low cloud amount.

Another is that midlevel clouds are more likely to occur if the low clouds types cumulonimbus and stratus are present, as shown in Table 3. These low clouds are indicative of convection (indeed, ''fractostratus and/or fractocumulus of bad weather'' is the low cloud type most frequently associated with tropical rain). Associations between the individual cloud types are more explicit about this connection. The thicker midlevel cloud types, namely, ''altocumulus (Ac) of a chaotic sky,'' ''altocumulus with turrets,'' ''double-layered Ac,'' ''Ac formed by the spreading out of Cu,'' and ''thick Ac,'' are primarily associated with the more substantial low cloud types indicative of convective conditions, such as ''cumulonimbus,'' ''cumulus and stratocumulus with bases at different levels,'' and ''bad-weather scud.''

The increased frequency with which midlevel cloud occurs as the low cloud amount increases is particularly pronounced for this convective region and can be seen in Fig. 5. From this figure, we find a middle cloud frequency of occurrence of 84% for all times when low clouds cover at least half of the celestial dome. From this we estimate that when the sky is completely obscured by low cloud, midlevel cloud is likely to occur 84% of the time. This is significantly higher than the similarly inferred estimate of 50% utilized within the middle cloud amount calculations of Warren et al. (1988). Midlevel cloud amount similarly increases with low cloud amount (results not shown), lending support to the sounding results of Fig. 4. This reflects the relatively large horizontal dimensions of stratus and cumulonimbus and the smaller horizontal dimensions of cumulus. These related inferences all reflect the association of midlevel clouds with the more convective low cloud types.

4. Possible causes for the 600–800-mb minimum

Both the soundings and the surface observations support the idea that convection is an important generating mechanism for midlevel cloud. The soundings furthermore imply that even within the presence of convection, cloud generation preferentially avoids the 600–800-mb layer. During the TOGA COARE IOP, deep convective activity was frequent (Chen et al. 1996; Gutzler et al. 1994), being supported by a generally conditionally unstable atmosphere, a high (>27°C) sea surface temperature, and an often moist boundary layer. Here we seek an explanation for the observed cloud vertical structure by examining how convection interacts with the middle tropical troposphere.

We utilize the buoyancy-sorting cloud model of Raymond and Blyth (1992). Within this model, an initial parcel constructed from the mean properties of the 950–1000-mb layer of the atmosphere is assumed to ascend through the troposphere, mixing at each level with nine different mixing fractions ranging from 0.1 to 0.9. In this manner a spectrum of multiple mixing events can be represented. The mixing events occur at all 5-mb pressure levels between cloud base (i.e., where the mixing ratio of the initial undilute parcel exceeds that of the environment) up to the highest level of neutral buoyancy for the initial parcel. These dilute parcels then move to their nearest level of neutral buoyancy and remain there; no overshooting is allowed to occur. As vapor condenses, the liquid water is initially kept within the parcel until a preestablished maximum value is reached, after which the water leaves as precipitation. Differing assumptions about the ice and precipitation microphysics (i.e., whether cloud particles are liquid or ice, and and how much liquid water remains carried within a parcel before it is precipitated out) will affect the detrainment, so results are shown for varying assumptions. Pressure gradient forces are not included in the model.

The model was applied to the Kapingamarangi soundings ($N = 485$). The relative humidity profile for this station is drier than the mean profile shown in Fig. 1 throughout most of the depth of the troposphere but most noticeably at lower altitudes. Soundings from this station contain a dry bias in the boundary layer that is thought to be caused by an air-conditioned launch. Reliable surface humidity measurements were not available with which to apply a correction. The initial model

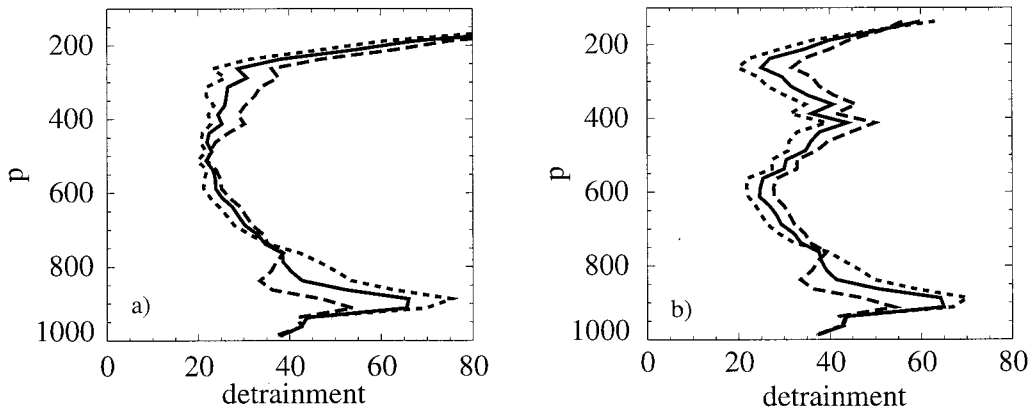

FIG. 6. Histogram of the outflow levels from the Raymond–Blyth model of the total ensemble of diluted parcels at Kapingamarangi, assuming (a) deposition at temperatures below 0°C and (b) liquid water condensation only. Dotted, solid, and dashed lines denote liquid water parcel maxima of 5, 3, and 1 g kg^{-1}, respectively.

parcel will possess a dry bias then, which may express itself within the model in decreased buoyancy. This may affect the proportional outflow occurring at different altitudes but leaves the central result, that more outflow occurs at locations with more stable layers, unaffected.

The detrainment is shown as a histogram of the outflow levels of the total ensemble of diluted parcels. In Fig. 6a, the mean detrainment assumes depositional growth of ice particles above the 0°C level while in Fig. 6b condensational growth of liquid particles only is assumed. Detrainments for three different maximum parcel liquid water amounts (1, 3, and 5 g kg^{-1}), representing different efficiencies for the formation and fallout of precipitation, are shown. These numbers span the range in maximum water loadings in model simulations of GATE (Global Atmospheric Research Program Atlantic Tropical Experiment) clouds (Ferrier and Houze 1989). The differing assumptions for cloud particle growth and precipitation efficiency all result in minimum detrainment at around 600 mb. In the more realistic case that includes the depositional growth of ice crystals, the increased latent heating enhances the parcel buoyancy and the detrainment minimum extends farther up the atmosphere. As the maximum liquid water carried within the parcel is increased, the parcel buoyancy decreases, leading to decreased detrainment at pressures below 750 mb and increased detrainment at pressures greater than 750 mb.

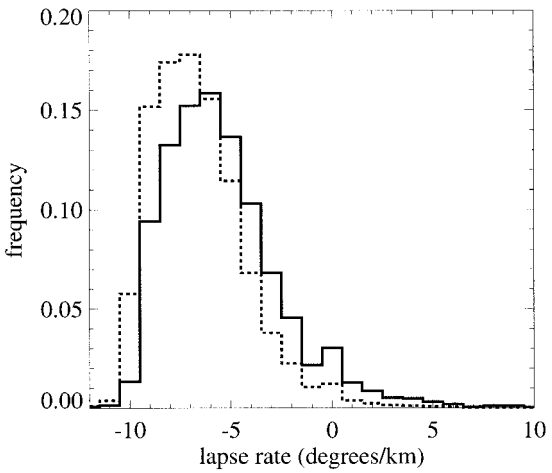

FIG. 7. Relative frequency of all the 10-mb layer lapse rates (dashed line) and of only those layers into which detrainment is occurring (solid line), up to 200 mb. Instantaneous freezing and a maximum liquid water parcel loading of 4 g kg^{-1} is assumed. Layers between 950 and 1000 mb, whose mean properties determine the initial parcel, are excluded.

Detrainment occurs preferentially into layers of decreasing buoyancy with height (Bretherton and Smolarkiewicz 1989; Ferrier and Houze 1989; Taylor and Baker 1991; Raymond and Wilkening 1982). Such layers can be regions of high stability. Using the model of Raymond and Blyth (1992) we obtain a preferential detrainment into layers with enhanced stability, shown here in Fig. 7. The solid line denotes the relative frequency of the 5-mb layer lapse rates into which detrainment is occurring, while the dashed line gives the relative frequency of all the layer lapse rates.

Layers of enhanced stability are not evenly distributed within the tropical atmosphere (Johnson et al. 1996; Mapes and Zuidema 1996). Rather, as shown in Fig. 8, such layers are more common around 800 mb and then again above 600 mb, with a minimum in between. The distribution of stable layers has this bimodal structure for all weather conditions (Fig. 17 of Johnson et al. 1996). If most of the detrainment is occurring into the stable layers, then less cloud material will be found between 600 and 800 mb. This is indeed what we see in Fig. 6, although the detrainment and stable-layer profiles do not entirely coincide. For example, most of the lower-level detrainment is occurring at around 900 mb instead of near the relative maximum in stable-layer frequency at 800 mb, reflecting the negative buoyancy of many of the lower parcels. At the lowest liquid water loading (1 g kg^{-1}), a secondary outflow

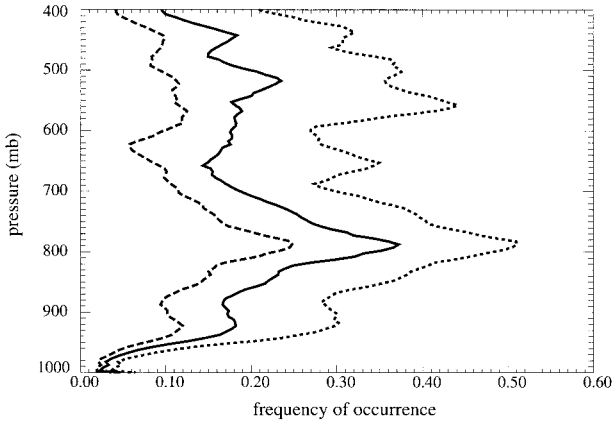

FIG. 8. Frequency of occurrence of stable layers at Kapinga. Stable layers with lapse rates exceeding $-5°$, $-4°$, and $-3°$C km^{-1} are indicated by a dotted, solid, and dashed line, respectively (cf. Fig. 17 of Johnson et al. 1996).

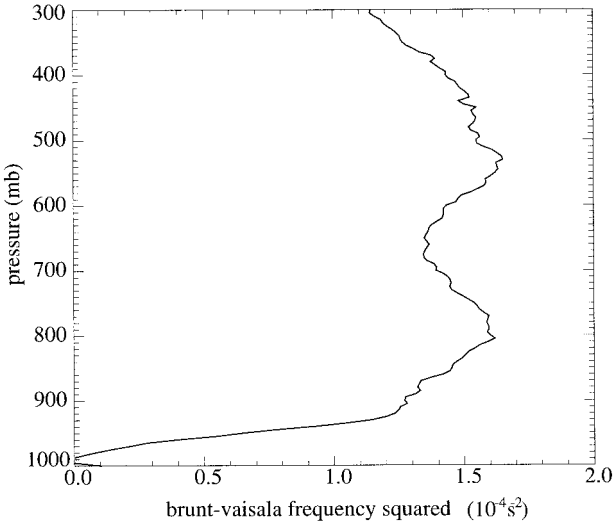

FIG. 9. The static stability parameter buoyancy frequency squared $N^2 \equiv (g/\theta)(\partial\theta/dz)$, where $\theta = T(p_0/p)^{R/c_p}$, T is temperature, R is the gas constant, c_p is the heat capacity, p is pressure in mb, and p_0 is 1000 mb. Values for T and p are for the COARE mean sounding.

maximum occurs at the 800-mb level, marking the trade wind inversion. Detrainment at around 550 mb is not particularly pronounced despite the enhanced frequency of stable layers at that level. When deposition is ignored (an ultimately unrealistic assumption given a mean freezing level of 565 mb), outflow at this level increases. It may be that initially liquid water will detrain at the subfreezing temperatures, after which the clouds glaciate and persist.

Although the preceding analysis has focused on the mean effect of individual soundings, the minimum in stability and detrainment occurring between 600 and 800 mb is ubiquitous and is a feature of the mean tropical atmosphere. The detrainment calculated from the mean sounding (not shown) is very similar to the mean detrainments shown in Fig. 6 and captures this minimum. The vertical distribution of stable layers shown in Fig. 8 can also be seen within the mean stability profile, shown here in Fig. 9. The mean tropical atmosphere is less stable between 600 and 800 mb than either above or below those levels, so that a parcel with enough buoyancy to reach 750 mb can continue on to 600 mb, unless inhibited by entrainment and precipitation.

5. Conclusions

We have shown 1) that a minimum in cloud coverage occurs between 600 and 800 mb according to sonde observations; 2) that this minimum occurs in all weather conditions; 3) that clouds existing between 800 and 400 mb are associated with overall convective, disturbed conditions, according to both surface and satellite observations; and 4) that this cloudiness minimum can be understood as a preferential detrainment into layers of enhanced stability that occur more frequently at altitudes below 750 mb and above 600 mb. The cloud distribution depicted in Fig. 3 finds support in a radar study of convection (Rickenbach and Rutledge 1998), which shows a large frequency of occurrence of radar echos with tops near 6 km (~500 mb) and a smaller maximum near 800 mb reflecting lightly precipitating tradelike cumulus. The pronounced peak at 950 mb and the smaller peak at 830 mb of Fig. 3 may reflect separate ''forced'' and ''active'' shallow cumulus populations (Johnson and Lin 1997). The cloud mininum occurs irrespective of the prevailing meteorological conditions, coincident with a stable layer distribution that is present in all weather states (Fig. 17 of Johnson et al. 1996). While a focus on the cloudy and stable layers highlights their association, both are so ubiquitous within the tropical atmosphere that a 700-mb minimum in relative humidity and static stability can be seen even within the mean tropical profiles and in the detrainment calculated from the mean profiles.

This attribute of the mean tropical atmosphere, then, is so general that the problem of explaining the tropical vertical cloud distribution is related to explaining the mean tropical temperature profile. This intriguing question is beyond the scope of this study, but the interaction of convection itself with the stratification must be a central element. The interaction can be a coupled process, as on the one hand, the detrainment of cloudy air will alter the stratification; but on the other hand, the stratification may well have resulted from prior convective processes such as shallow cloud top detrainment near 800 mb, melting in midlevels, or from an emanating gravity wave from more distant convection (Johnson et al. 1996). Downdrafts in deep convection may also play an important role in setting the environmental stratification (Mapes 1997).

This study is a continuation of work presented in Mapes and Zuidema (1996), who suggested that the humidity transition layers they studied are also preferred levels for clouds. The suggestion of Mapes and Zuidema (1996) finds support here in the results of a simple cloud buoyancy-sorting model, wherein a boundary layer par-

cel is mixed with environmental air at all fractions and heights and the mixtures allowed to move to their level of neutral buoyancy. Regions of enhanced stability are indeed preferred for the detrainment of cloudy air, with nonequilibrium themodynamics possibly playing a role in furthering the generation of midlevel clouds. Once a midlevel cloud is generated, it can be maintained for some time through radiative cooling of the upper part and warming below (e.g., Starr and Cox 1985; Lilly 1988) and will contribute to the thin midlevel layer cloud population frequently seen by surface observers.

Much still remains to be known about the distribution of midlevel tropical clouds. The simplicity of the Raymond–Blyth model means that the detrainment profiles may not be quantitatively correct, so that one intriguing further avenue of research would be to specialize the Raymond–Blyth model for TOGA COARE conditions. Cumulus ensemble models, which diagnostically generate cloud fields consistent with observed large-scale tropical budget data, can possibly provide the most comprehensive depiction of tropical vertical cloud distributions. Some such models show a cloudiness minimum at the 700-mb level, while others do not. These models may not necessarily resolve shallow cumulus, so that the results at low levels may be resolution dependent (e.g., Fig. 10 of Xu and Randall 1995), but this issue remains to be addressed. The motivation for understanding the distribution of the midlevel clouds is strong, as these in turn affect radiative and latent heating profiles and thereby the dynamics associated with the warm pool region.

Acknowledgments. This research was supported by NSF Grant ATM-9525801 and the Department of Energy Atmospheric Radiation Program. The author thanks Dr. Judith Curry for providing the freedom and support to pursue this research and for comments that much improved the manuscript. I thank Brian Mapes for his introduction to the Raymond–Blyth model and its possibilities, for stimulating interest in this research, and for providing encouragement and valuable comments. In addition the carefully considered comments of Dr. Richard Johnson and two anonymous reviewers helped add depth and breadth to this article. Thanks are also extended to Dr. David Raymond for his generosity in making the cloud model code available.

REFERENCES

Betts, A. K., C. S. Bretherton, and E. Klinker, 1995: Relation between mean boundary-layer structure and cloudiness at the R/V *Valdivia* during ASTEX. *J. Atmos. Sci.,* **52,** 2752–2762.

Bretherton, C. S., and P. K. Smolarkiewicz, 1989: Gravity waves, compensating subsidence and detrainment around cumulus clouds. *J. Atmos. Sci.,* **46,** 740–759.

Chen, S. S., R. A. Houze Jr., and B. E. Mapes, 1996: Multiscale variability of deep convection in relation to large-scale circulation in TOGA COARE. *J. Atmos. Sci.,* **53,** 1380–1409.

Ferrier, B. S., and R. A. Houze Jr., 1989: One-dimensional time-dependent modeling of GATE cumulonimbus convection. *J. Atmos. Sci.,* **46,** 330–351.

Flatau, P. J., R. L. Walko, and W. R. Cotton, 1992: Polynomial fits to saturation vapor pressure. *J. Appl. Meteor.,* **31,** 1507–1513.

Garand, L., C. Grassotti, J. Halle, and G. Klein, 1992: On differences in radiosonde humidity—Reporting practices and their implications for numerical weather prediction and remote sensing. *Bull. Amer. Meteor. Soc.,* **73,** 1417–1423.

Gutzler, D. S., G. N. Kiladis, G. A. Meehl, K. M. Weickmann, and M. Wheeler, 1994: The global climate of December 1992–February 1993. Part II: Large-scale variability across the tropical western pacific during TOGA COARE. *J. Climate,* **7,** 1606–1622.

Hahn, C. J., S. G. Warren, J. London, R. M. Chervin, and R. Jenne, 1982: Atlas of simultaneous occurrence of different cloud types over the ocean. NCAR Tech. Note TN-201+STR, 212 pp. [Available from National Center for Atmospheric Research, Boulder, CO 80307-3000.]

——, ——, and ——, 1994: Edited synoptic cloud reports from ships and land stations over the globe, 1982–1991. NDP026B, 47 pp. [Available from Carbon Dioxide Information Analysis Center, Oak Ridge National Laboratory, Oak Ridge, TN 37831-6335.]

Johnson, R. H., and J. A. Dickey, 1996: Effects of convection on the atmospheric boundary layer as revealed by TOGA COARE Sounding Data. Preprints, *Eighth Conf. on Air–Sea Interaction,* Atlanta, GA, Amer. Meteor. Soc., J29–J32.

——, and X. Lin, 1997: Episodic trade wind regimes over the western Pacific warm pool. *J. Atmos. Sci.,* **54,** 2020–2034.

——, P. E. Ciesielski, and K. A. Hart, 1996: Tropical inversions near the 0°C level. *J. Atmos. Sci.,* **53,** 1838–1855.

Lilly, D. K., 1988: Cirrus outflow dynamics. *J. Atmos. Sci.,* **45,** 1594–1605.

Mapes, B., 1997: Mutual adjustment of mass flux and stratification profiles. *The Physics and Parameterization of Moist Convection,* R. K. Smith, D. J. Raymond, and M. Miller, Eds., Kluwer Academic, 399–412.

——, and P. Zuidema, 1996: Radiative-dynamical consequences of dry tongues in the tropical troposphere. *J. Atmos. Sci.,* **53,** 620–638.

Miller, E., 1993: TOGA COARE integrated sounding system data report—Volume I, surface and sounding data. NCAR SSSF Rep., 41 pp. [Available from National Center for Atmospheric Research, Boulder, CO 80307-3000.]

Nash, J., J. B. Elms, and T. J. Oakley, 1995: Relative humidity sensor performance observed in recent international radiosonde comparisons. Preprints, *Ninth Symp. on Meteorological Observations and Instrumentation,* Charlotte, NC, Amer. Meteor. Soc., 43–48.

Parsons, D., and Coauthors, 1994: The integrated sounding system: Description and preliminary observations from TOGA COARE. *Bull. Amer. Meteor. Soc.,* **75,** 553–568.

Paukkunen, A., 1995: Sensor heating to enhance reliability of radiosonde humidity measurement. Preprints, *Ninth Symp. on Meteorological Observations and Instrumentation,* Charlotte, NC, Amer. Meteor. Soc., 65–69.

Ramaswamy, V., and V. Ramanathan, 1989: Solar absorption by cirrus clouds and the maintenance of the tropical upper troposphere thermal structure. *J. Atmos. Sci.,* **46,** 2293–2310.

Randall, D. A., Harshvardhan, D. A. Dazlich, and T. G. Corsetti, 1989: Interactions among radiation, convection, and large-scale dynamics in a general circulation model. *J. Atmos. Sci.,* **46,** 1944–1970.

Raymond, D. J., and M. H. Wilkening, 1982: Flow and mixing in New Mexico mountain cumuli. *J. Atmos. Sci.,* **39,** 2211–2228.

——, and A. M. Blyth, 1992: Extension of the stochastic mixing model to cumulonimbus clouds. *J. Atmos. Sci.,* **49,** 1968–1983.

Rickenbach, T. M., and S. A. Rutledge, 1998: Convection in TOGA COARE: Horizontal scale, morphology, and rainfall production. *J. Atmos. Sci.,* in press.

Rossow, W. B., and L. C. Garder, 1993: Validation of ISCCP cloud detections. *J. Climate,* **6,** 2370–2393.

Sherwood, S. C., V. Ramanathan, T. P. Barnett, M. K. Tyree, and E. Roeckner, 1994: Response of an atmospheric general circulation model to radiative forcing of tropical clouds. *J. Geophys. Res.,* **99,** 20 829–20 845.

Sheu, R.-S., J. A. Curry, and G. Liu, 1997: Vertical stratification of tropical cloud properties as determined from satellite. *J. Geophys. Res.,* **102,** 4231–4245.

Starr, D. O'C., and S. K. Cox, 1985: Cirrus clouds. Part II: Numerical experiments on the formation and maintenance of cirrus. *J. Atmos. Sci.,* **42,** 2682–2694.

Taylor, G. R., and M. B. Baker, 1991: Entrainment and detrainment in cumulus clouds. *J. Atmos. Sci.,* **48,** 112–121.

Wang, J., and W. B. Rossow, 1995: Determination of cloud vertical structure from upper air observations. *J. Appl. Meteor.,* **34,** 2243–2258.

Warren, S. G., C. J. Hahn, J. London, R. M. Chervin, and R. L. Jenne, 1988: Global distribution of total cloud cover and cloud type amounts over the ocean. NCAR/TN-317 + STR, 42 pp. + 170 maps. [Available from National Center for Atmospheric Research, Boulder, CO 80307-3000.]

Webster, P. J., and R. Lukas, 1992: TOGA COARE: The Coupled Ocean–Atmosphere Response Experiment. *Bull. Amer. Meteor. Soc.,* **73,** 1377–1416.

White, A. B., and C. W. Fairall, 1996: Shipboard measurements of convection during COARE. Preprints, *Eighth Conf. on Air–Sea Interaction,* Atlanta, GA, Amer. Meteor. Soc., J16–J19.

——, ——, and J. B. Snider, 1995: Surface-based remote sensing of marine boundary-layer cloud properties. *J. Atmos. Sci.,* **52,** 2827–2838.

Xu, K.-M., and D. A. Randall, 1995: Impact of interactive radiative transfer on the macroscopic behavior of cumulus ensembles. Part I: Radiation parameterization and sensitivity tests. *J. Atmos. Sci.,* **52,** 785–799.